Electrical control of Kondo effect and superconducting transport in a side-gated InAs quantum dot Josephson junction

Y. Kanai,[1,*] R. S. Deacon,[1] A. Oiwa,[1,2,3] K. Yoshida,[2] K. Shibata,[4] K. Hirakawa,[3,4,5] and S. Tarucha[1,2,5]
[1]*Department of Applied Physics and QPEC, The University of Tokyo, 7-3-1 Hongo, Bunkyo-ku 113-8656, Japan*
[2]*Quantum Spin Information Project, ICORP, JST, Atsugi-shi, Kanagawa 243-0198, Japan*
[3]*JST CREST, 4-1-8 Hon-cho, Kawaguchi-shi, Saitama 332-0012, Japan*
[4]*Institute of Industrial Science, The University of Tokyo, 4-6-1 Komaba, Meguro-ku, Tokyo 153-8505, Japan*
[5]*INQIE, The University of Tokyo, 4-6-1 Komaba, Meguro-ku, Tokyo 153-8505, Japan*
(Received 7 April 2010; revised manuscript received 30 June 2010; published 11 August 2010)

We measure the nondissipative supercurrent in a single InAs self-assembled quantum dot (QD) coupled to superconducting leads. The QD occupation is both tuned by a back-gate electrode and lateral side gate. The geometry of the side gate allows tuning of the QD-lead tunnel coupling in a region of constant electron number with an appropriate orbital state. Using the side-gate effect we study the interplay between Kondo correlations and superconducting pairing on the QD, observing a decrease in the supercurrent when the Kondo temperature is reduced below the superconducting energy gap in qualitative agreement with theoretical predictions.

DOI: 10.1103/PhysRevB.82.054512 PACS number(s): 74.45.+c, 74.50.+r, 73.63.Kv, 73.23.Hk

I. INTRODUCTION

Devices which combine the gate tunability of semiconductor quantum dots (QDs) with nondissipative superconducting transport are desirable for very sensitive and controllable coherent switching devices[1,2] and the study of interplay between Kondo physics and the superconducting proximity effect.[3–25] The Kondo effect arises at low temperatures, below a characteristic Kondo temperature (T_K), when a single localized spin is screened by a high order spin-flip cotunneling with a reservoir of spins. In QDs the resulting many-body Kondo state lifts the Coulomb blockade giving rise to a characteristic zero-bias conductance anomaly.[26,27] In the conventional *s*-wave superconducting state electrons form spin singlet Cooper pairs. The important energy scales for the interaction between Kondo singlet state and superconductivity are broadly captured in the scaling parameter $t_K=k_BT_K/\Delta$ where Δ is the superconducting energy gap. For $t_K \gg 1$ the local magnetic moment of the unpaired electron spin on the QD is screened by the Kondo effect and the ground state of the system is a Kondo singlet state. In this regime an enhanced supercurrent due to the Kondo effect has been predicted theoretically.[4,12,15] However, for $t_K \ll 1$ the Kondo state is suppressed by the lack of low energy excitations in the superconducting energy gap and the system ground state is a degenerate (so-called magnetic) doublet state. To date most experimental efforts to elucidate this phase transition have been unable to systematically control the physical parameters which determine t_K due to the limited tunability of the devices studied. Recently Eichler *et al.*[21] used the dependence of T_K on the energy level of a carbon nanotube QD controlled using a back-gate electrode to study the supercurrent in different regimes. In the present paper, we demonstrate that t_K may be smoothly controlled by tuning the tunnel coupling by a side-gate, which is placed laterally to an InAs self-assembled QD. The sidegate performance is very effective for uncapped InAs self-assembled QDs as the lateral confinement tuned by the sidegate is weak relative to that in nanowire or nanotube devices. The parameter t_K is tuned through control of the tunnel coupling between QD energy levels and the source and drain electrodes. The technique allows the study of supercurrent for a range of t_K while maintaining both the charging state of the QD and control of the QD energy level using a backgate electrode (for example maintaining the half-filling condition). When t_K is tuned through $t_K \sim 1$ we observe a dramatic change in the superconducting transport indicating the phase transition between Kondo singlet and magnetic doublet states.

To date works on the interplay of Kondo and proximity effect have focused on either the dissipative transport or the nondissipative supercurrent. For low biases within the subgap transport region the dissipative transport current is carried by multiple Andreev reflections[28] (MAR). MAR resonances occur when a sequence of Andreev reflections connect the high density of states at the edge of the superconducting energy gap. Subgap transport MAR resonances have been shown to be substantially altered by the single electron states of a QD[28–30] and the Kondo effect.[17–19] Observation of the supercurrent in QD Josephson junctions presents a greater challenge, which has been tackled in a number of recent studies.[1,20–22] In weakly coupled devices where the doublet state dominates the reversal of the supercurrent or π-junction has been demonstrated[1,20,22] in good agreement with theoretical predictions.[3,31] In the strongly coupled Kondo regime the supercurrent has been analyzed through current-biased *V-I* characteristics in QD Josephson junctions[21] and discussed in terms of the zero-bias peak in differential conductance measurements[23] with evidence of enhanced critical currents when $t_K > 1$. In this report we study both the dissipative MAR transport and nondissipative supercurrents, using a side-gate effect to electrically tune the scaling parameter t_K.

II. EXPERIMENTAL DETAILS

Devices were fabricated with a single uncapped InAs self-assembled QD with diameter and height of $\sim$100 nm and $\sim$20 nm, respectively. Conventional *e*-beam lithography and

 ©2010 The American Physical Society

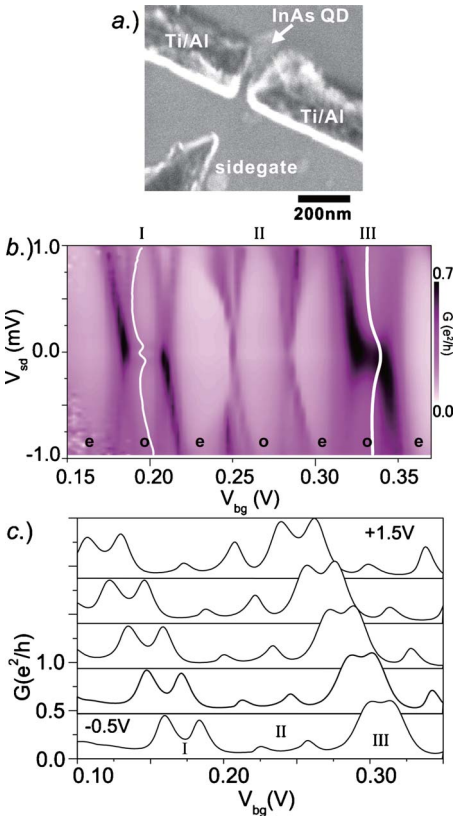

FIG. 1. (Color online) (a) Scanning electron microscope image of the sample studied. (b) Normal state stability diagram ($B=200$ mT, $V_{sg}=0$ V). Even (e) and odd (o) electron occupations are indicated. White traces show the Kondo zero-bias conductance anomaly in the center of regions I and III. (c) Normal state Coulomb peaks at $V_{sd}=0$ V for a range of applied V_{sg}. Curves from top to bottom are $V_{sg}=+1.5$ to -0.5 V in -0.5 V steps. Measurements are offset for clarity.

e-beam evaporation techniques were used to deposit two Titanium/Aluminum (5/100 nm) electrodes with a nanogap separation of less than 30 nm [Fig. 1(a)]. Prior to evaporation the surface oxide is removed with a six second etch in a 40% buffered hydroflouric acid solution to ensure transparent contacts. The back gate is a degenerately Si-doped GaAs layer buried 300 nm below the sample surface. The side-gate is placed about 200 nm away from the QD laterally. Additional device fabrication details can be found in references.[19,32] Transport measurements were performed in a ^{3}He-^{4}He dilution refrigerator with base temperature $\sim$30 mK. The differential conductance was measured using conventional lock-in techniques with an ac excitation of $V_{ac}\sim 3$ μV. For measurement of the supercurrent a four-terminal setup with current-bias was applied.

III. RESULTS

We first discuss measurements of the normal state transport and characterization of relevant device parameters in a range of charge states. The influence of the side-gate on normal state device parameters will then be discussed in Sec. III B, following which the influence on superconducting transport is shown in Sec. IV.

A. Normal state

Figure 1(b) shows a false colorplot of the differential conductance ($G=dI/dV_{sd}$) taken by sweeping the back-gate V_{bg} and source-drain voltage V_{sd} under an applied magnetic field of 200 mT and side-gate bias $V_{sg}=0$ V. The applied field exceeds the Al lead critical field ($B_c\sim 150$ mT) such that the leads are in the normal state. In the V_{bg} range measured we identify three regimes with odd electron occupation, labeled as I, II, and III. The charging energy U is roughly estimated from the width of the Coulomb diamonds to be 2.1, 2.9, and 2.0 meV in regions I, II and III respectively. We evaluate the back-gate leverarm, which relates V_{bg} to the energy in the QD,[19] to be $\alpha_{bg}\sim 0.09$ eV/V. Regions I and III exhibit Kondo zero-bias conductance anomalies which are split and broadened by Zeeman energy, respectively, (Landé g-factor $|g^*|=6.1\pm 0.2$ and 5.1 ± 0.3 for regions I and III, respectively). In region III we estimate T_K from the full width at half maximum (FWHM$=2k_BT_K$) of Lorentzian fits to the Kondo feature[26] with a linear background subtraction. By subtracting Zeeman energy from the FWHM a nominal Kondo temperature of $T_K=2.6\pm 0.3$ K ($t_K\sim 1.4$) is evaluated. In region I we observe the Kondo feature is already split at $B=200$ mT indicating Zeeman energy exceeds T_K, giving an upper limit of $T_K<0.82\pm 0.03$ K ($t_K<0.44$). No Kondo feature is observed in region II indicating that T_K is much lower than the measurement temperature.

B. Action of the side gate

We will now focus on the effect of the side gate on the normal state transport. Coulomb oscillations in the normal state for $V_{sd}=0$ V and a range of V_{sg} are shown in Fig. 1(c). Coulomb peaks are shifted toward lower V_{bg} as V_{sg} is increased with an evaluated leverarm of $\alpha_{sg}\sim 0.025\alpha_{bg}$. We observe that V_{sg} also alters the lineshape of the Coulomb peaks. To characterize the influence of the side-gate we extract estimates of both the asymmetry in source (S) and drain (D) lead tunnel couplings ($\chi=\Gamma_{S,D}/\Gamma_{D,S}$) and the total tunnel coupling ($\Gamma=\Gamma_S+\Gamma_D$) by fitting the even valley part of the Coulomb oscillation peaks using a Lorentzian expression following the method used by Jorgensen *et al.*[33] Following this method we fit Coulomb peaks with the expression[34]

$$G=\frac{e^2}{h}\frac{4\Gamma_S\Gamma_D}{\Gamma^2}\frac{(\tilde{\Gamma}/2)^2}{\varepsilon_d^2+(\tilde{\Gamma}/2)^2}, \tag{1}$$

where the total tunnel rate on/off of the QD is $\hbar/\Gamma$, $\Gamma=\Gamma_S+\Gamma_D$ and $\tilde{\Gamma}=1.36\Gamma$. The QD energy level ε_d is determined using the back gate leverarm $\alpha_{bg}=\Delta V_{sd}/\Delta V_{bg}$ evaluated for each charge state from the charge stability diagram. To avoid the influence of the Kondo zero-bias anomaly we only fit data in the even occupation regime (except for region II where no Kondo zero-bias anomaly is observed). Results of the average tunnel coupling $\langle\Gamma\rangle$ and average tunnel coupling asymmetry $\langle\chi\rangle$ evaluated for the two Coulomb peaks in all

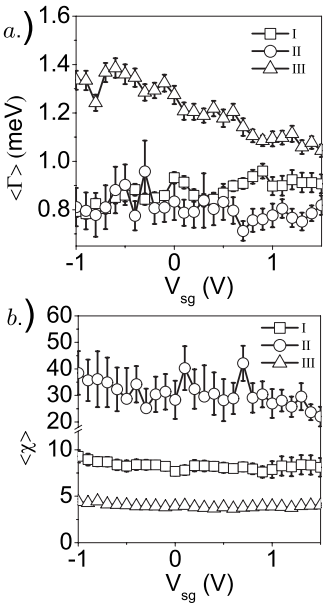

FIG. 2. (a) Summary of normal state $\langle\Gamma\rangle$ as a function of V_{sg} evaluated from fits of Coulomb peaks with Eq. (1) in regions I, II, and III. (b) Summary of $\langle\chi\rangle$ as a function of V_{sg} for regions I, II, and III.

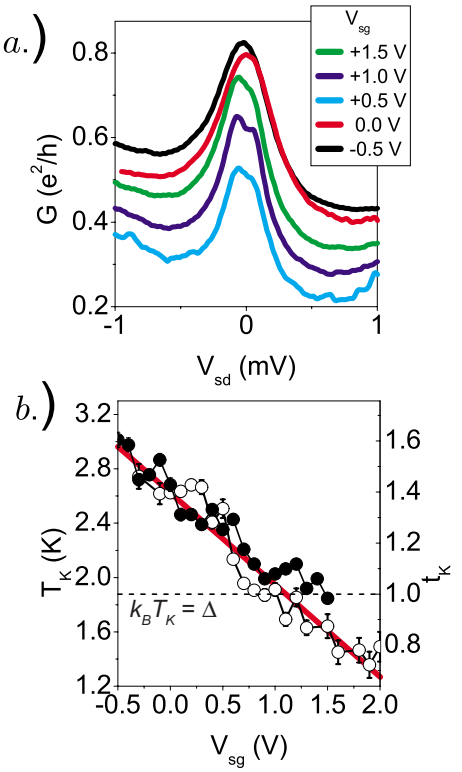

FIG. 3. (Color online) (a) Normal state (B=200 mT) Kondo zero-bias anomaly in the center of region III for a range of V_{sg}. Traces from bottom to top (V_{sg}=+2.0 V to V_{sg}=0.0 V are each offset by $+0.1e^2/h$ for clarity. (b) T_K evaluated in region III from the FWHM of the Kondo feature at B=200 mT (○) and calculated from $\langle\Gamma\rangle$ and $U\sim 2$ meV using Eq. (2) (●). The horizontal dashed line indicates $k_BT_K=\Delta$. The solid line indicates a linear best fit to the FWHM data.

three regions are plotted in Figs. 2(a) and 2(b), respectively. Values of $\langle\chi\rangle$ for regions I and III are found to be fairly constant while region II displays a decrease in $\langle\chi\rangle$ with increasing V_{sg} which accounts for the increase in peak conductance of the fourth Coulomb peak observed in Fig. 2(a). Only in region III is an appreciable change in $\langle\Gamma\rangle$ observed. In all regions we observe no significant change in $|g|$-factor or U when V_{sg} is altered.

Figure 3(a) shows $G(V_{sd})$ traces in the center of region III for a range of V_{sg}. As V_{sg} is increased the feature narrows and two Zeeman split peaks become more apparent indicating that T_K decreases relative to the Zeeman energy. As no appreciable change in $|g|$ is found this indicates a clear reduction in T_K. We quantitatively estimate T_K from the FWHM of the Kondo zero-bias anomaly[19] in region III for a range of V_{sg} in Fig. 3(b). We observe a linear change in T_K as V_{sg} is applied. The dependence of T_K on Γ in the center of the odd electron occupation region is well formulated as[35]

$$T_K \sim \tfrac{1}{2}\sqrt{U\Gamma}\exp(-\pi U/4\Gamma). \qquad (2)$$

The observed decrease in T_K evaluated from the FWHM with increasing V_{sg} is consistent with the decrease calculated from Eq. (2) using $\langle\Gamma\rangle$ evaluated in Fig. 2(a). This indicates that the control of T_K using the side-gate is achieved through tuning of the tunnel coupling. In regions I and II both $\langle\Gamma\rangle$ and U remain relatively constant when V_{sg} is applied and we therefore observed no noticeable effect on T_K. The tunnel coupling Γ is determined by the effective overlap between lead states and the wave function of the confined electrons.[32] We expect that the side-gate modulates the lateral confinement and displaces the electron wave function, resulting in a change in Γ. The influence of the side-gate is therefore highly dependent on specific symmetry of the orbital state and the corresponding expansion of the wave function, which accounts for the different behavior in regions I, II, and III. We conclude that in region III the parameter t_K may be tuned in the range $t_K\sim 1.5\rightarrow 0.8$.

IV. SUPERCONDUCTING STATE

We now focus on the transport when the applied magnetic field is removed and the leads are in the superconducting state. In Fig. 4(b), we present a false color plot of $G(V_{sd},V_{bg})$ focusing on a bias window about the superconducting energy gap for B=0 mT. For comparison the normal state data from Fig. 1(b) is included in Fig. 4(a). In the even electron occupation regime where Coulomb blockade dominates [Fig. 4(d)] prominent resonances at $|eV_{sd}|=2\Delta$ are attributed to direct quasiparticle tunneling between the high density of states at the edge of the superconducting gap in the two leads. A weaker feature at $|eV_{sd}|=\Delta$ is attributed to resonant single Andreev reflections or the first-order MAR resonance [see Fig. 4(c)]. We evaluate that $\Delta\sim 162$ μeV from V_{sd} at the resonances [Figs. 4(b) and 4(d)]. In odd electron occupation regions the spectrum of MAR features may be renormalized by the Kondo effect resulting in enhanced first-order MAR features at the expense of single quasiparticle

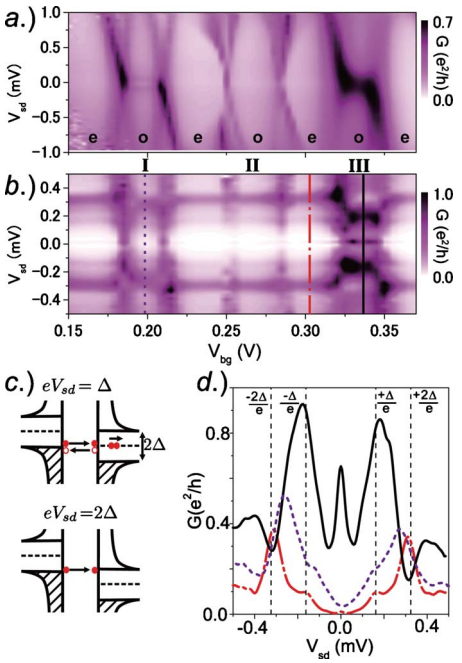

FIG. 4. (Color online) (a) Normal state stability diagram (B =200 mT, V_{sg}=0 V). Even (e) and odd (o) electron occupations are indicated. (b) Superconducting state stability diagram (B =0 mT, V_{sg}=0 V). (c) Energy schematics for the first-order MAR (eV_{sd}=Δ) and single quasiparticle tunneling resonances (eV_{sd} =2Δ). (d) Superconducting state $G(V_{sd})$ traces for even electron occupation Coulomb blockade (V_{bg}=0.3 V, red dot/dashed line), the center of region III (V_{bg}=0.335 V, solid line) and the center of region I (V_{bg}=0.2 V, purple dotted line).

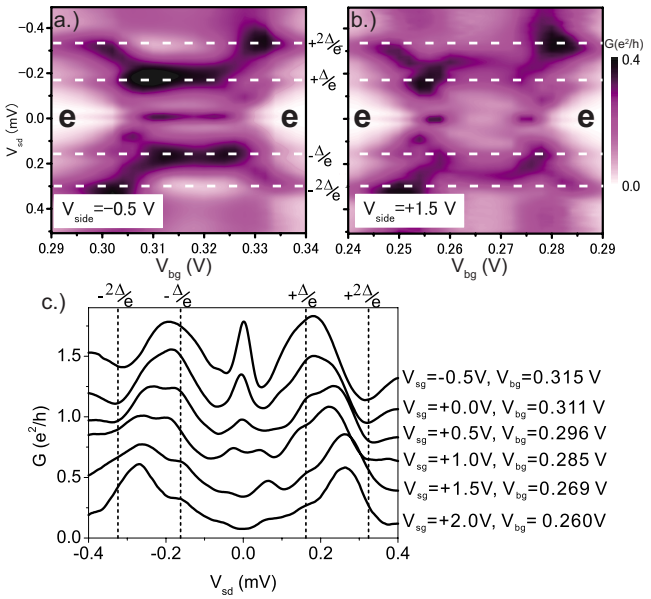

FIG. 5. (Color online) Plots of $G(V_{sd}, V_{bg})$ displaying the subgap transport resonances in region III for V_{sg}=−0.5 V (a) and V_{sg} =+1.5 V (b). Horizontal lines indicate bias for quasiparticle tunneling resonance $|eV_{sd}|$=2Δ and first-order MAR $|eV_{sd}|$=Δ. Even (e) occupation regions are identified. (c) Plot of $G(V_{sd})$ in the center of region III (half filling) for a range of V_{sg}. Traces from bottom to top are offset by $+0.2e^2/h$ for clarity.

tunneling.[17–19] Of the regions considered only region III displays enhancement of first-order MAR relative to the 2Δ features, likely due to the higher T_K. A sharp zero-bias conductance peak is observed in both even occupation regions and regions II and III, however this feature is absent in region I. In regions II and III we can eliminate the Kondo zero-bias anomaly as an origin of the superconducting state zero-bias peak because the magnetic field dependence does not show Zeeman splitting. The zero-bias peak can therefore be regarded as a signature of supercurrent through the device.[23] A significant supercurrent feature is observed only in region III providing evidence of enhancement for high-normal state T_K.[4] In the sections, which follow we discuss the effect of the side-gate on both the dissipative transport and nondissipative supercurrent. We first discuss the arguably more interesting transport in region III (Sec. IV A) where the side-gate has a significant effect before looking briefly at the influence in regions I and II (Sec. IV B).

A. Region III

We now focus on the superconducting transport in region III when the side-gate is used to tune t_K through unity. Figure 5(a) shows a false color plot of differential conductance around region III for V_{sg}=−0.5 V (a) and +1.5 V (b), focusing on the subgap transport resonances described earlier. While the even occupation regions display similar subgap transport resonances when V_{sg}=+1.5 and V_{sg}=−0.5 V, the odd occupation region displays pronounced differences. The zero-bias conductance peak is observed for V_{sg}=−0.5 V but not for V_{sg}=+1.5 V, indicating a suppression of the supercurrent when V_{sg} is increased. Figure 5(c) displays plots of $G(V_{sd})$ at the center of the region III for a range of V_{sg}. The magnitude of the zero-bias peak is gradually reduced and disappears at around $V_{sg}\sim+0.8$ V. When the zero-bias peak diminishes a pair of small resonances are observed near V_{sd}=0. These resonances may be attributed to higher order MAR. We also observe a distinct shift in the most prominent transport resonance from the first-order MAR feature at $|eV_{sd}|$=Δ to an intermediate feature between $|eV_{sd}|$=2Δ and $|eV_{sd}|$=Δ. Note also that the minima at $|eV_{sd}|$=2Δ are suppressed as V_{sg} is increased. Viewed in the context of recent studies of the interplay between MAR and the Kondo effect[17–19] we attribute the pronounced change in the resonances to a reduction of the influence of Kondo effect on the spectrum of MAR resonances. We note similarity between the subgap resonances in region III for high V_{sg} (indicating low T_K) with those observed in region I [shown in Fig. 9(a)] where $t_K<0.44$.

We analyze the transport further using a four terminal current bias measurement to study the supercurrent. When measuring the supercurrent in the junction we must consider the dissipation in the surrounding circuit,[36] which determines the characteristics of the V-I curves.[2,21,22,37] The nonlinear dynamics of the circuit are intuitively captured in the modified resistively capacitively shunted junction (RCSJ) model.[36] We use the modified RCSJ model of Ref. 2 which accounts for lead capacitances and resistances by assuming the circuit shown in Fig. 6(a). Here C_J and R_J are the Joseph-

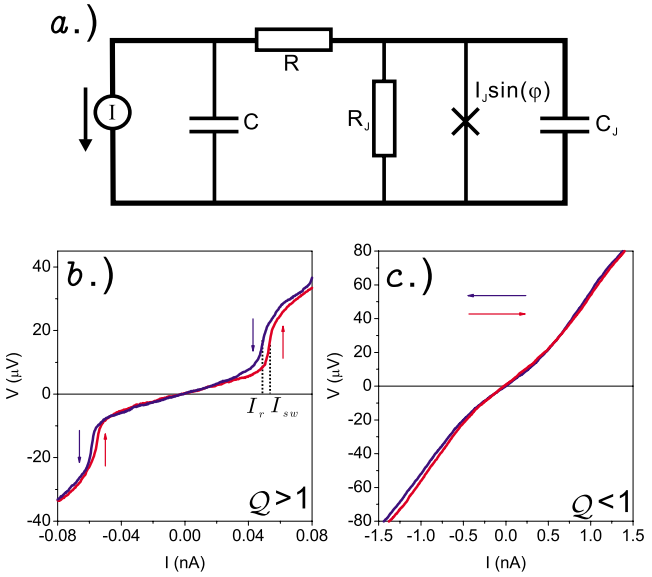

FIG. 6. (Color online) (a) RCSJ circuit. (b) Example of underdamped behavior at V_{sg}=+1.0 V and V_{bg}=0.258 V (even occupation regime near region III) where $\mathcal{Q}\sim 5.5$. (c) Example overdamped behavior at V_{sg}=0.0 V and V_{bg}=0.29 V (inside region III) where $\mathcal{Q}\sim 1$.

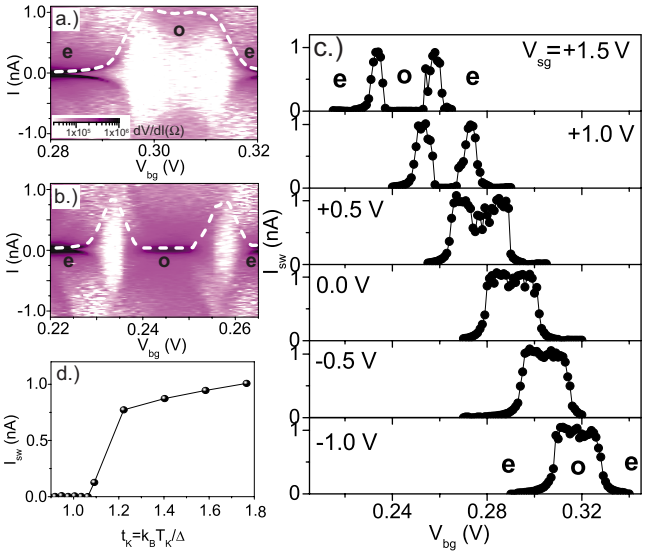

FIG. 7. (Color online) Plot of dV/dI for four terminal I-bias measurements in region III with V_{sg}=−0.5 V (a) and V_{sg}=+1.5 V (b). Dashed white lines indicate the trend of I_{sw}. (c) $I_{sw}(V_{bg})$ in region III for a range of V_{sg}. (d) $I_{sw}(t_K)$ for the center of region III (half filling). t_K is estimated from the linear fit in Fig. 3(b). Even (e) and odd (o) occupation is indicated.

son junction capacitance and resistance respectively. R and C represent the "on chip" extrinsic circuit resistance and capacitance due to contacting leads and pads. The dynamics of the system are captured in the quality factor ($\mathcal{Q}$) defined as

$$\mathcal{Q}=\frac{1}{\omega_p\left(RC+\frac{\hbar}{2e}\frac{1}{I_cR_J}\right)}, \tag{3}$$

where ω_p is the "plasma frequency" given as

$$\omega_p=\sqrt{\frac{2eI_c}{\hbar\left(C\left(1+\frac{R}{R_J}\right)+C_J\right)}}, \tag{4}$$

and I_c indicates the intrinsic junction critical current in the absence of fluctuations. The quality factor indicates the stability of the phase across the junction to fluctuations in the bias which may be caused by a noisy environment. In the limit $\mathcal{Q}\ll 1$ the dissipation is strong and phase changes across the junction are suppressed resulting in an overdamped junction, which displays no hysteresis in V-I traces. If $\mathcal{Q}\gg 1$ the phase changes across the junction are fast compared with the dissipation and the junction is underdamped. In this limit the switching between supercurrent and normal branches is a stochastic process and hysteresis is observed in V-I traces. Note however that hysteresis may also be attributed to thermal effects.[38]

We evaluate $C_J\sim e^2/2U\sim 20$ aF, $C\sim 30$ pF from the area of ohmic bonding pads and $R\sim 100$ Ω from Ti/Au bridge electrodes used to contact the desired nanogap.[39] We qualitatively evaluate the relative evolution of the junctions intrinsic critical current using a "switching current" (I_{sw}), taken as the current value at the maximum differential resistance. In the calculation of $\mathcal{Q}$ we assume the I_c is given by I_{sw}. I_{sw} is influenced by the dissipation of the extrinsic circuit and is expected to be significantly reduced from the intrinsic critical current due to thermal fluctuations. In the Coulomb blockade regime high R_J results in a nominally underdamped junction for which the V-I trace is hysteretic with sharp switching between superconducting and normal branches, Fig. 6(b). In contrast near Coulomb peaks and areas with strong Kondo effect (region III) low R_J leads to a nominally overdamped/critically damped junction with no hysteresis, Fig. 6(c). In this regime we attribute smooth V-I traces to an overdamped Josephson junction with a finite resistance in the supercurrent branch from thermal phase diffusion.[40] The overdamped region results in a broad zero-bias conductance peak in the voltage bias measurements as observed in Fig. 4(b).

We plot the four-terminal differential resistance (dV/dI) as a function of V_{bg} and current (I) for V_{sg}=−0.5 V and V_{sg}=+1.5 V in Figs. 7(a) and 7(b), respectively. White dashed lines indicate the evaluated I_{sw}. In Fig. 7(a) where V_{sg}=−0.5 V, I_{sw} is high in the odd occupation region and small but nonzero in the even occupation regions where Coulomb blockade dominates. Figure 7(c) shows the evolution of $I_{sw}(V_{bg})$ for a range of V_{sg}. In good agreement with the V-bias measurements we find that supercurrent feature is reduced to zero in the odd electron occupation region when V_{sg} is high. Numerical renormalization group[11,12,43,44] and functional renormalization group[15] studies predict a significant drop in absolute I_c when the device is tuned to the magnetic doublet regime. The overall trend of $I_{sw}(V_{bg})$ on V_{sg} shown in Fig. 7(d) therefore qualitatively matches the scenario of a phase transition between a Kondo dominated singlet state to a degenerate magnetic doublet. In Fig. 7(d), we plot the switching current as a function of t_K evaluated at the half

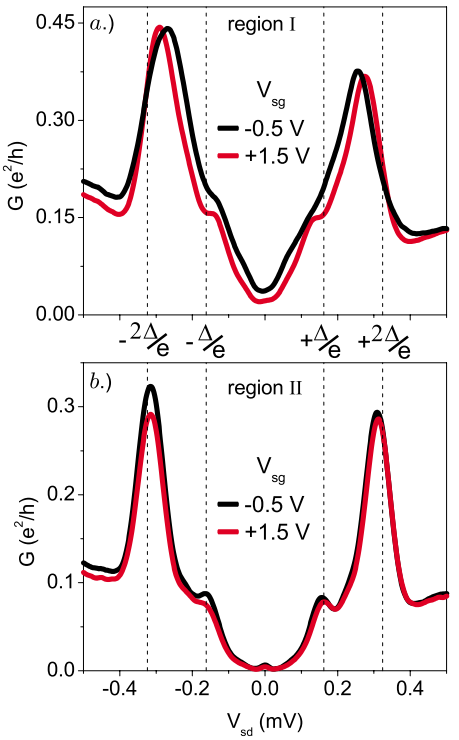

FIG. 8. (Color online) (a) $G(V_{sd})$ in the center of region I for $V_{sg}=-0.5$ V and +1.5 V. (b) $G(V_{sd})$ in the center of region II for $V_{sg}=-0.5$ V and +1.5 V. Vertical dashed lines indicate bias conditions for first-order MAR and single quasiparticle tunneling resonances.

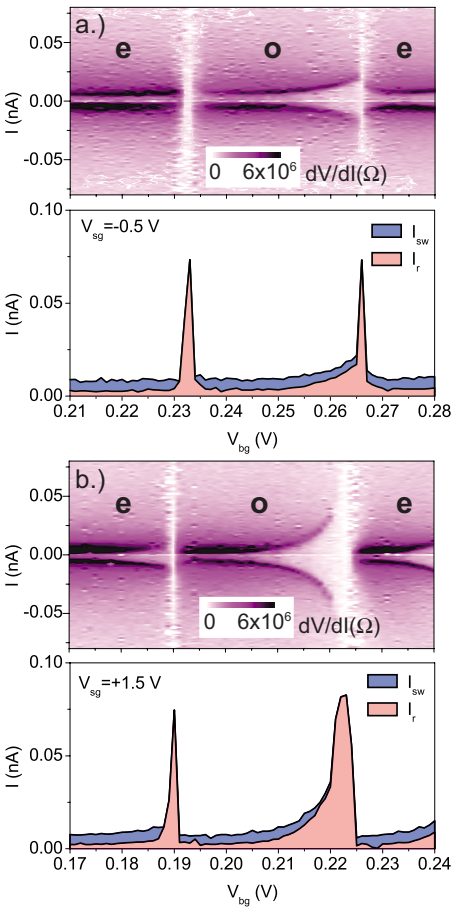

FIG. 9. (Color online) (a) *I*-bias measurements of region II with $V_{sg}=-0.5$ V. The false color plot of dV/dI is generated from traces with *I* swept from positive to negative. (b) *I*-bias measurements of region I with $V_{sg}=+1.5$ V. The false color plot of dV/dI is generated from traces with *I* swept from positive to negative. Even (e) and odd (o) occupation regions are identified.

filling condition in the center of the Kondo region. In the magnetic doublet regime ($t_K<1$) the supercurrent is strongly suppressed by Coulomb blockade while in the Kondo singlet regime ($t_K>1$) the supercurrent may be enhanced by the Kondo effect. In other studies[1,22] the low supercurrent in the magnetic doublet (π-junction) regime (when $t_k \ll 1$) has been measured, however in the device considered here no supercurrent branch is observed implying that coherent processes are overcome by dissipation in the circuit and thermal fluctuations due to a poorly screened electromagnetic environment. The singlet-doublet transition is observed at $t_K \sim 1.1$ in good agreement with the disappearance of the zero-bias peak in voltage bias measurements shown in Fig. 5(c). While the parameter t_K broadly captures the behavior of the device the specifics of the system ground state are in fact determined by multiple parameters including the tunnel coupling with left and right lead, the charging energy and superconducting gap. The ability to tune T_K with the sidegate while maintaining control of the QD energy level using the backgate allows study of I_c vs. t_K at the half-filling position in the center of the Kondo region for which numerical renormalization group studies are known to provide a good description of the system.[15] Choi *et al.*[12] used the numerical renormalization group to calculate I_c as a function of t_K and predicted the transition at $t_K \sim 0.5$. For $t_K>0.5$ a saturation of I_c was predicted. This explains the observed trend of I_{sw} shown in Fig. 7(d). Siano and Egger[14] applied the Quantum Monte Carlo method to predict a transition at $t_K \sim 1.1$. Our experimental result is in good qualitative agreement with the predicted features in both of these studies. Discrepancies may arise from the nonideal nature of real devices in which tunnel coupling is asymmetric and extrinsic environmental effects may dominate.

B. Region I and II

Finally for completeness we briefly discuss the effect of the side-gate in regions I and II. Figure 8 displays plots of $G(V_{sd})$ in the center of regions I and II for low and high V_{sg}. Both regions display prominent single quasiparticle tunnelling resonances at $|eV_{sd}| \sim 2\Delta$ and weak first-order MAR features. Note that in region II we observe a zero-bias conductance peak indicating the presence of a supercurrent. Compared with region III the application of V_{sg} has negligible effect on the subgap resonances, as may be expected from the negligible effect on $\langle\Gamma\rangle$ observed in § III B [Fig. 2(a)]. Region I does display a small shift of the direct quasiparticle tunnelling feature to a lower source-drain bias [Fig. 8(a)]. Similar albeit larger shifts were observed in region III [Fig. 5(c)] as T_K was reduced. The small shift in region I may

therefore indicate some reduced influence from weak Kondo effect for higher V_{sg}.

Four contact current bias measurements reveal no evidence of supercurrent features in region I but a supercurrent branch is identified in region II for small currents. Figures 9(a) and 9(b) show I-bias measurements in region II for low and high V_{sg}, respectively. As region II predominantly displays underdamped behavior we record both the switching current I_{sw} and the re-entrant or retrapping current I_r, the comparison of which give an indication of the hysteresis. While I_{sw} is unchanged in the center of region II we note an increase in I_{sw} near the second Coulomb peak when V_{sg} is increased from $V_{sg}=-0.5$ V to $V_{sg}=+1.5$ V. In the underdamped regime the critical current (I_c) in the noninteracting system has been shown to scale as[2,41]

$$\frac{I_c}{I_0} = \left(1 - \sqrt{1 - \frac{G_N h}{2e^2}}\right)^{3/2}, \tag{5}$$

where $I_0=2e\Delta/\hbar$ and G_N is the normal state conductance. Depairing due to strong electron-electron interaction has been predicted[3] to cause a further significant suppression of I_c, which most likely accounts for the small switching currents observed in the measurement. The observed increase in I_{sw} around the second Coulomb peak in region II may be attributed to a decrease in the tunnel coupling asymmetry χ [as shown in Fig. 2(b)] which results in a higher normal state conductance G_N and thus critical current.

V. CONCLUSIONS

We study transport through a single self-assembled InAs quantum dot gated with both back and side-gate electrode. The side-gate is demonstrated to allow limited tuning of Kondo temperature through tuning of tunnel coupling in a region of constant electron number. This technique is used to elucidate the effect of Kondo correlations on both the supercurrent and subgap dissipative transport around the phase transition between magnetic double and Kondo singlet states. The onset of the transition was observed at $t_K=k_BT_K/\Delta \sim 1.1$. The side-gate technique presented here can offer broad tunability of the dot parameters, such as tunnel coupling, its asymmetry, and the resultant Kondo temperature. We note that the sidegate technique may also allow tuning of other device parameters which are sensitive to the orbital states such as Landé g-factor and spin orbit interaction.[42]

ACKNOWLEDGMENTS

We acknowledge valuable discussions with A. Oguri and Y. Tanaka. We acknowledge financial support from JSPS (Y.K.), Grant No. P07328 (R.S.D.), Grant-in-Aid for Scientific Research S (Grant No. 19104007) and A (Grant No. 21244046) (A.O.) and Innovative Areas (Grant No. 21102003), JST strategic Int. Coop. Program, FIRST program, and QuEST under Grant No. HR-001-09-1-0007 and QuEST program (Grant No. BAR-0824) (S.T.).

*kanai@meso.t.u-tokyo.ac.jp

[1] J. van Dam, Y. Nazarov, E. Bakkers, S. de Franceschi, and L. Kouwenhoven, Nature (London) **442**, 667 (2006).
[2] P. Jarillo-Herrero, J. van Dam, and L. Kouwenhoven, Nature (London) **439**, 953 (2006).
[3] E. Vecino, A. Martin-Rodero, and A. Levy Yeyati, Phys. Rev. B **68**, 035105 (2003).
[4] L. Glazman and K. Matveev, Sov. Phys. JETP **46**, 659 (1989).
[5] T. Meng, S. Florens, and P. Simon, Phys. Rev. B **79**, 224521 (2009).
[6] Y. Avishai, A. Golub, and A. D. Zaikin, Phys. Rev. B **63**, 134515 (2001).
[7] Y. Avishai, A. Golub, and A. D. Zaikin, Phys. Rev. B **67**, 041301 (2003).
[8] L. Dell'Anna, A. Zazunov, and R. Egger, Phys. Rev. B **77**, 104525 (2008).
[9] A. A. Clerk, V. Ambegaokar, and S. Hershfield, Phys. Rev. B **61**, 3555 (2000).
[10] J. Bauer, A. Oguri, and A. Henson, J. Phys. Condens. Matter **19**, 486211 (2007).
[11] A. Oguri, Y. Tanaka, and A. Hewson, J. Phys. Soc. Jpn. **73**, 2494 (2004).
[12] M.-S. Choi, M. Lee, K. Kang, and W. Belzig, Phys. Rev. B **70**, 020502(R) (2004).
[13] Y. Tanaka, A. Oguri, and A. C. Hewson, New J. Phys. **9**, 115 (2007).
[14] F. Siano and R. Egger, Phys. Rev. Lett. **93**, 047002 (2004).
[15] C. Karrasch, A. Oguri, and V. Meden, Phys. Rev. B **77**, 024517 (2008).
[16] M. R. Buitelaar, T. Nussbaumer, and C. Schönenberger, Phys. Rev. Lett. **89**, 256801 (2002).
[17] T. Sand-Jespersen, J. Paaske, B. M. Andersen, K. Grove-Rasmussen, H. I. Jørgensen, M. Aagesen, C. B. Sørensen, P. E. Lindelof, K. Flensberg, and J. Nygård, Phys. Rev. Lett. **99**, 126603 (2007).
[18] A. Eichler, M. Weiss, S. Oberholzer, C. Schönenberger, A. Levy Yeyati, J. C. Cuevas, and A. Martin-Rodero, Phys. Rev. Lett. **99**, 126602 (2007).
[19] C. Buizert, A. Oiwa, K. Shibata, K. Hirakawa, and S. Tarucha, Phys. Rev. Lett. **99**, 136806 (2007).
[20] J. Cleuziou, W. Wersdorfer, V. Bouchiat, T. Ondarcuhu, and M. Monthioux, Nat. Nanotechnol. **1**, 53 (2006).
[21] A. Eichler, R. Deblock, M. Weiss, C. Karrasch, V. Meden, C. Schönenberger, and H. Bouchiat, Phys. Rev. B **79**, 161407(R) (2009).
[22] H. I. Jørgensen, T. Novotny, K. Grove-Rasmussen, K. Flensberg, and P. Lindelof, Nano Lett. **7**, 2441 (2007).
[23] K. Grove-Rasmussen, H. Jorgensen, and P. Lindelof, New J. Phys. **9**, 124 (2007).
[24] M. Gräber, T. Nussbaumer, W. Belzig, and C. Schönenberger, Nanotechnology **15**, S479 (2004).
[25] R. S. Deacon, Y. Tanaka, A. Oiwa, R. Sakano, K. Yoshida, K. Shibata, K. Hirakawa, and S. Tarucha, Phys. Rev. B **81**, 121308(R) (2010).

[26] D. Goldhaber-Gordon, H. Shtrikman, D. Mahalu, D. Abusch-Magder, U. Meirav, and M. A. Kastner, Nature (London) **391**, 156 (1998).
[27] Y. Igarashi, M. Jung, M. Yamamoto, A. Oiwa, T. Machida, K. Hirakawa, and S. Tarucha, Phys. Rev. B **76**, 081303 (2007).
[28] M. R. Buitelaar, W. Belzig, T. Nussbaumer, B. Babić, C. Bruder, and C. Schönenberger, Phys. Rev. Lett. **91**, 057005 (2003).
[29] A. Levy Yeyati, J. C. Cuevas, A. Lopez-Davalos, and A. Martin-Rodero, Phys. Rev. B **55**, R6137 (1997).
[30] G. Johansson, E. N. Bratus, V. S. Shumeiko, and G. Wendin, Phys. Rev. B **60**, 1382 (1999).
[31] B. I. Spivak and S. A. Kivelson, Phys. Rev. B **43**, 3740 (1991).
[32] M. Jung, T. Machida, K. Hirakawa, S. Komiyama, T. Nakaoka, S. Ishida, and Y. Arakawa, Appl. Phys. Lett. **87**, 203109 (2005).
[33] See the supporting material of Ref. 22 and theoretical work of König *et al.* (Ref. 34).
[34] J. König, J. Schmid, H. Schoeller, and G. Schön, Phys. Rev. B **54**, 16820 (1996).
[35] F. D. M. Haldane, Phys. Rev. Lett. **40**, 416 (1978).
[36] M. Tinkham, *Introduction to Superconductivity* (McGraw-Hill, New York, 1996).
[37] G. Liu, Y. Zhang, and C. N. Lau, Phys. Rev. Lett. **102**, 016803 (2009).
[38] H. Courtois, M. Meschke, J. T. Peltonen, and J. P. Pekola, Phys. Rev. Lett. **101**, 067002 (2008).
[39] K. Shibata, C. Buizert, A. Oiwa, K. Hirakawa, and S. Tarucha, Appl. Phys. Lett. **91**, 112102 (2007).
[40] G.-L. Ingold, H. Grabert, and U. Eberhardt, Phys. Rev. B **50**, 395 (1994).
[41] C. W. J. Beenakker, Phys. Rev. B **46**, 12841 (1992).
[42] S. Takahashi, R. S. Deacon, K. Yoshida, A. Oiwa, K. Shibata, K. Hirakawa, Y. Tokura, and S. Tarucha, Phys. Rev. Lett. **104**, 246801 (2010).
[43] K. Satori, H. Shiba, O. Sakai, and Y. Shimizu, J. Phys. Soc. Jpn. **61**, 3239 (1992).
[44] O. Sakai, Y. Shimizu, H. Shiba, and K. Satori, J. Phys. Soc. Jpn. **62**, 3181 (1993).